



## Article

# Functionalization of Silica SBA-15 with [3-(2-Aminoethylamino)Propyl] Trimethoxysilane in Supercritical CO<sub>2</sub> Modified with Methanol or Ethanol for Carbon Capture

Yolanda Sánchez-Vicente <sup>1,2,\*</sup> , Lee Stevens <sup>3</sup>, Concepción Pando <sup>4</sup> and Albertina Cabañas <sup>4</sup> 

<sup>1</sup> Department of Mechanical & Construction Engineering, Faculty of Engineering and Environment, Northumbria University, Newcastle upon Tyne NE1 8ST, UK

<sup>2</sup> Department of Chemical Engineering, Imperial College London, South Kensington Campus, London SW7 2AZ, UK

<sup>3</sup> Low Carbon Energy and Resources Technologies Research Group, Faculty of Engineering, University of Nottingham, Nottingham NG7 2RD, UK; lee.stevens@nottingham.ac.uk

<sup>4</sup> Department of Physical Chemistry, Universidad Complutense de Madrid, 28040 Madrid, Spain; pando@quim.ucm.es (C.P.); a.cabanas@quim.ucm.es (A.C.)

\* Correspondence: yolanda.vicente@northumbria.ac.uk; Tel.: +44-191-227-3533

Received: 28 September 2020; Accepted: 5 November 2020; Published: 6 November 2020



**Abstract:** The CO<sub>2</sub> adsorption process using amine-grafted silica is a promising technology for reducing the CO<sub>2</sub> emissions from the power and industry sectors. In this work, silica SBA-15 was functionalized using [3-(2-aminoethylamino)propyl] trimethoxysilane (AEAPTS) in supercritical CO<sub>2</sub> (scCO<sub>2</sub>) modified with 10% mol methanol or ethanol. The functionalization experiments were carried out at 323 K and 12.5 MPa, and with reaction times of 2 and 3 h. The molar fraction of AEAPTS in scCO<sub>2</sub> plus 10% mol alcohol ranged from  $0.5 \times 10^{-3}$  to  $1.8 \times 10^{-3}$ . It was found that as the molar fraction of AEAPTS increased, the amino-grafting density steadily rose, and the pore volume, surface area and pore size of the functionalized silica SBA-15 also decreased gradually. The scCO<sub>2</sub> functionalization method was compared to the traditional toluene method. The diamine-SBA-15 prepared in the scCO<sub>2</sub> process shows a slightly lower amine-grafting density but a higher surface area and pore volume than the ones obtained using the traditional method. Finally, the excess CO<sub>2</sub> adsorption capacity of the materials at different temperatures and low pressure was measured. The diamine-silica SBA-15 displayed moderate excess CO<sub>2</sub> adsorption capacities, 0.7–0.9 mmol·g<sup>-1</sup>, but higher amine efficiency, ca. 0.4, at 298 K, due to the chemisorption of CO<sub>2</sub>. These findings show that diamine-grafted silica for post-combustion capture or direct air capture can be obtained using a media more sustainable than organic solvents.

**Keywords:** mesoporous silica; surface functionalization; supercritical fluids; CO<sub>2</sub> adsorption; diamine

## 1. Introduction

Global energy consumption is increasing rapidly as a result of population and economic growth, particularly in the emerging market economies [1]. Presently, more than 80 per cent of the world's primary energy consumption is based on fossil fuels, even with the dramatic development of renewable energies. CO<sub>2</sub> emissions have increased as a result of burning fossil fuels, and they are responsible for climate change, which has become a significant international concern. A global action plan to limit the global average temperature rise to well below 2 °C by 2100 was agreed in Paris in 2015 [2]. The decarbonisation process will require a combination of technologies. Among these, carbon capture

and storage (CCS) is an essential technology in the short- and medium-term to reduce anthropogenic CO<sub>2</sub> emissions, primarily from the power and industry sectors, protecting energy systems. Another benefit of CCS technology in comparison with renewable energies in the power sector is that it can be retrofitted into multiple industrial processes such as natural gas, mining, hydrogen production, oil extraction, steel and cement production [3].

The most advanced technology existing for CO<sub>2</sub> capture is chemical absorption utilizing primary, secondary, tertiary and cyclic amines, as well as other blends. However, the CO<sub>2</sub> absorption process exhibits many drawbacks, including high energy demands for sorbent regeneration and corrosion of the equipment. The adsorption process is seen as an alternative to carbon capture solvent methods, with several benefits, including a wide range of operating conditions, minimizing the energy needs, safer solid waste and preventing corrosion [4]. A broad range of solids can be used to adsorb CO<sub>2</sub>, and each class has its advantages and disadvantages [5]. They can be divided into the following eight groups: zeolites and microporous silicates, aluminium phosphates, carbons, other porous oxides, metal–organic frameworks (MOFs), covalent organic frameworks (COFs), amine-containing solids and other sorbents (lithium zirconates, CaO, MgO, hydrotalcites etc.). Zeolites and activated carbons capture CO<sub>2</sub> via physical adsorption and consequently are typically hindered in the presence of water [6]. Stability in the presence of moisture may be a problem for most of the MOFs [7]. Metal oxides (CaO, MgO etc.), lithium zirconates and hydrotalcites capture CO<sub>2</sub> via chemical reactions [8]. Amine-grafted mesoporous silica has been extensively studied among the different adsorbent materials for CCS. These materials have excellent operational performance, good stability against water, high surface areas and high CO<sub>2</sub> selectivity since they adsorb CO<sub>2</sub> by the formation of the carbamate salt [9]. In general, a higher amine loading on mesoporous silica will result in more significant adsorption of CO<sub>2</sub> [10]. Amine-silica solids are mainly designed to adsorb CO<sub>2</sub> at low pressure as in post-combustion or direct air capture processes [11]. Pressure swing adsorption (PSA) and temperature swing adsorption (TSA) are the two principal operating methods for CO<sub>2</sub> adsorption processes. CO<sub>2</sub> is desorbed by depressurization in the PSA process, while in the TSA process, the desorption occurs by the increasing temperature. TSA is more likely to be a suitable approach for CO<sub>2</sub> adsorption on amine-grafted silica since the CO<sub>2</sub> molecules are primarily chemically adsorbed on the materials [12–15].

Amine compounds can be grafted on the silica surface by condensation reactions between alkoxysilane and the silanol groups on the silica surface [16]. This reaction, known as the silanization reaction, is typically performed in solution using anhydrous organic solvents, for example, toluene, to obtain densely derived silane layers [17]. Several disadvantages associated with this process are the production of a large volume of organic solvent waste and side reactions such as solution oligomerization. Supercritical carbon dioxide (scCO<sub>2</sub>) has lately been considered a sustainable alternative to the organic solvents for amine surface modification [18]. The supercritical approach provides essential benefits for the functionalization of porous materials since the supercritical medium allows the transfer of precursors to the internal surface of the pores without structural loss due to low viscosity, very low surface tension and moderate diffusivity. Surface modification reactions in scCO<sub>2</sub> are faster than in organic solvents, primarily due to the excellent transport properties [19]. Furthermore, CO<sub>2</sub> is non-toxic, non-flammable, cheap and relatively inert, and CO<sub>2</sub> and alcohol are the only by-products of the process. Due to all these benefits, the scCO<sub>2</sub> process is a sustainable solution for surface functionalization [20,21]. Besides, CO<sub>2</sub> can be removed from the material by reducing the pressure, and the gaseous CO<sub>2</sub> can then be recycled. Most of the CO<sub>2</sub> used in the supercritical process can be obtained as a by-product in industrial chemical processes such as ammonia production or the CO<sub>2</sub> recovered in carbon capture processes. Therefore, this approach does not lead to an increase in the amount of CO<sub>2</sub> in the atmosphere. On the contrary, supercritical CO<sub>2</sub> processes might provide a method for recovering some part of the CO<sub>2</sub> industrial emissions [22].

A specific drawback associated with the scCO<sub>2</sub> solvent for the silanization reaction of aminosilane is that the secondary and primary amines present in the silane agent can react with CO<sub>2</sub> and form the carbamate salt, which is insoluble in scCO<sub>2</sub>. Various strategies have been explored to solve this issue in

the literature. Since carbamate formation can be reversed at high temperatures and moderate pressures, López-Aranguren et al. modified the surface of four silica supports with aminosilanes at 373 and 408 K and 7.5 and 10 MPa [23]. Moreover, in our previous work, Sanchez-Vicente et al. [18] carried out the functionalization of silica SBA-15 with 3-aminopropyltrimethoxysilane (3APTS) in scCO<sub>2</sub> modified with 10% mol ethanol. The role of the 10% mol ethanol in the mixture was the solubilization of the possible aminoalkylcarbamate salt produced by the reaction between the amine group of 3APTS and CO<sub>2</sub>. Moreover, we investigated the grafting of tertiary amines into the mesoporous silica surface in scCO<sub>2</sub>, since the CO<sub>2</sub> only reacts with tertiary amines if water is present [19].

In this work, we investigated the amine surface functionalization of silica SBA-15 with [3-(2-aminoethylamino)propyl]trimethoxysilane (AEAPTS) in scCO<sub>2</sub> modified with ethanol or methanol at 323 K and 12.5 MPa. The chemical structures of AEAPTS and SBA-15 are shown in Figure 1. The AEAPTS was chosen as a grafting agent because it has a secondary amine and a primary amine. Therefore, the number of amines per total weight of material would be higher, and that could increase the CO<sub>2</sub> adsorption capacity. The formed carbamate salt was solubilized in scCO<sub>2</sub> by adding methanol or ethanol as a cosolvent, as was proposed in our previous work [18]. The selected temperature and pressure for performing the reaction were based on our earlier studies of the phase behaviour of similar systems [18,24,25]. The reaction mixture under those selected conditions may be an expanded liquid. The specific properties of expanded liquids are very similar to the supercritical fluid ones, including their low viscosity and surface tension as well as high diffusivity [26]. The silanization reaction in scCO<sub>2</sub> was compared to the conventional method using toluene. In addition to the non-toxicity of CO<sub>2</sub>, we proved that the scCO<sub>2</sub> procedure could be conducted in a far lower time than the traditional approach using organic solvents. Finally, the sorption efficiency of materials at low CO<sub>2</sub> pressures was tested to determine their potential as CO<sub>2</sub> adsorbent materials.

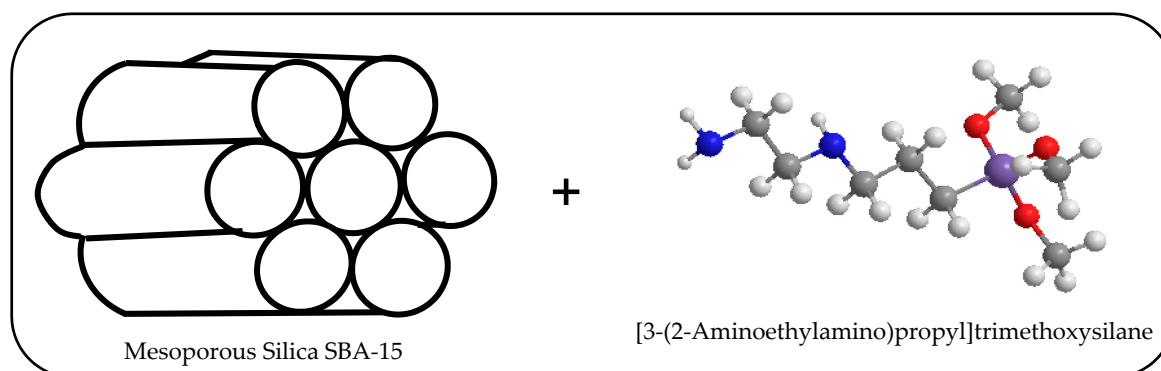


**Figure 1.** Schematic representation of the mesoporous silica SBA-15 and 3D chemical structure of the [3-(2-aminoethylamino)propyl]trimethoxysilane used in the silanization reaction. Atom colour code: nitrogen: blue; hydrogen: white; carbon: grey; oxygen: red; and silicon: purple.

## 2. Materials and Methods

### 2.1. Materials

CO<sub>2</sub> (purity > 99.99%) was obtained from Air Liquide. Tetraethylorthosilicate (TEOS, 99 + % pure), poly(ethyleneglycol)-block-poly(propylene glycol)-block-poly(ethyleneglycol) (Mw = 5800) (PEO-PPO-PEO), [3-(2-Aminoethylamino)propyl]trimethoxysilane (AEAPTS), ethanol (>99.5% pure, 0.5% water), and toluene (>99.5% pure) were supplied by Sigma-Aldrich, and methanol (99.99% pure), by Fisher. The materials were used as received. Mesoporous silica SBA-15 was prepared following a similar method to that reported by Zhao et al. [27]. In a representative experiment, 4.0 g of PEO-PPO-PEO was dissolved in 120 g of a 2 M HCl solution and 30 g of water, and then, the solution was stirred at 308 K. Afterward, 8.5 g of TEOS was added into the mixture with agitation at 313 K for 20 h. Then, the solution was aged without agitation at 373 K for a further 12 h. The solid

powder was filtered, washed with ethanol several times and calcined in air for 6 h at 823 K. Before the functionalization experiments, the mesoporous SBA-15 was not thermally treated or activated. The quantity of water adsorbed on the silica SBA-15 surface was roughly 5% wt, determined by TGA.

## 2.2. Functionalization of Silica SBA-15 with AEAPTS in $scCO_2$ Modified with ca. 10% Mol Alcohol

The functionalization of silica SBA-15 with AEAPTS using  $scCO_2$  plus ca. 10% mol alcohol was performed using the experimental methodology described previously [18,19]. A 65 cm<sup>3</sup> custom-made stainless-steel high-pressure reactor was used to conduct the experiments. The SBA-15 mesoporous silica was wrapped in filter paper and placed on the upper section of the reactor. A glass vial containing the ethanol/methanol + AEAPTS solution was placed at the bottom of the reactor. In a standard experiment, a specific amount of ethanol/methanol + AEAPTS solution was used to treat about 105 mg of SBA-15. The concentration of the solution was in molar excess relative to the silanol contained on the surface of SBA-15 silica (3.7 OH nm<sup>-2</sup>) [28]. Once the reactants were located into the reactor, the vessel was closed and heated to the required temperature using a silicone heating tape (Omegalux SRT051-040) joined to a proportional integral derivative (PID) temperature controller (Micromega, CN77322 model). The temperature was measured using a type J calibrated thermocouple. Then, a high-pressure syringe pump (Isco, Inc. Model 260D, Nebraska, USA) was used to fill the reactor with  $CO_2$  at the desired pressure, which was measured with a pressure transducer (Gems). The reactor was also fitted with a safety valve (Swagelok). To reach the homogeneous phase, a magnetic stirrer was employed to mix the reactants. During the reaction, the stability of the temperature and pressure was estimated to be  $\pm 2$  K and  $\pm 0.5$  MPa, respectively. After 3 or 2 h, a needle valve was used to depressurize the vessel for 15 min. Then, the reactor was cooled down and the diamino-modified silica was collected. Finally, the samples were filtered, washed with methanol or ethanol and dried for 24 h in a natural convection oven at 373 K to eliminate  $CO_2$  from the carbamate salt and potential traces of ethanol or methanol [29].

## 2.3. Conventional Functionalization of Silica SBA-15 with AEAPTS in Toluene

The conventional silanization of the silica SBA-15 was conducted according to the description in the literature [29]. Around 200 mg of SBA-15 silica, 1.5 g of AEAPTS and 50 cm<sup>3</sup> of toluene were loaded into a two-neck round-bottom glass flask fitted to a condenser. A hot plate with a temperature controller, an external temperature probe and stirring were then used to heat the silicon oil bath in which the glass flask was immersed. The reaction took place under a nitrogen atmosphere for 24 h at 323 K with gentle stirring. Subsequently to the silanization, the amine-grafted SBA-15 silica was filtered and washed with copious quantities of toluene and then ethanol. Finally, the sample was dried for 24 h in a natural convection oven at 373 K.

## 2.4. Material Characterization

The amine-grafted SBA-15 was characterized using thermogravimetric analysis (TGA), elemental analysis (EA) and  $N_2$  adsorption–desorption isotherms at 77 K. A TA Q-600 instrument was used to perform the TGA. Samples were heated up to 1073 K at 10 K min<sup>-1</sup> under nitrogen flow. A LECO CHNS-932 microanalyzer was utilized to conduct the elemental analysis. The uncertainties in the EA were %C  $\pm$  0.26, %H  $\pm$  0.24 and %N  $\pm$  0.25. ASAP-2020 equipment from Micrometrics was employed to perform the adsorption/desorption  $N_2$  isotherms at 77 K. The samples were degassed at 393 K for 3 h, before the adsorption tests. The surface areas were measured using the BET equation ( $S_{BET}$ ) for a  $P/P_0$  range from 0.05 to 0.25. The volume of the pore ( $V_p$ ) was estimated as the quantity of liquid nitrogen adsorbed at  $P/P_0$  at 0.95 [30]. The pore size distributions were determined using the Barrett–Joyner–Halenda (BJH) model for a cylindrical porous material and using the statistical thickness Kelvin equation. The volume of the micropore was calculated using the t-plot method ( $V_{\mu p}$ ). Low-angle XRD patterns of the silica SBA-15 before the surface modification with diaminosilane

were obtained using a aSAXS Kratky camera from HECUS-BRAUN with a PANalytical PW3830 X-ray generator.

### 2.5. Excess Carbon Dioxide Adsorption

A thermogravimetric analyser, TA Q-500, was used to measure low-pressure excess CO<sub>2</sub> adsorption. Around 15 mg of each sample was heated at 20 K min<sup>−1</sup> from 298 to 378 K under N<sub>2</sub> flow [14]. The sample was kept for 45 min at 378 K to remove moisture and then cooled at 10 K min<sup>−1</sup> to 298 K. The gas intake was switched from N<sub>2</sub> to CO<sub>2</sub> and kept isothermic for 90 min, and then, the temperature gradually rose up to 453 K at a speed of 0.25 K min<sup>−1</sup>. The capacity to adsorb CO<sub>2</sub> was calculated from the mass change of the sample in CO<sub>2</sub>. The effects of the changes in gas viscosity, density and buoyancy were corrected by measuring the response of an empty platinum crucible by the same method. The mass accuracy in the equipment is about 0.1%.

## 3. Results

### 3.1. Functionalization of Silica SBA-15 with AEAPTS

The functionalization of silica SBA-15 with AEAPTS was performed in scCO<sub>2</sub> modified with ca. 10% mol methanol or 10% mol ethanol. The performed experiments are provided in Table 1. In this study, silica SBA-15 was selected as a support because of its high surface area, large pore volumes, tuneable uniform pore sizes and ease of functionalization and characterization. Moreover, mesoporous silica SBA-15 has recently shown better amine-grafting ability than other mesoporous silica such as MCM-41, since the pore sizes and wall thicknesses of the SBA-15 are greater than those of the other supports [5,20]. SBA-15 consists of regular hexagonal arrays of cylindrical mesopores interconnected by smaller micro- and mesopores (see Figure 1). The low-angle XRD pattern of the substrate is shown in Figure 2. The first peak was allotted to the planes (100) and occurred at ca. 0.90 2θ values. Although the peaks (110) and (200) are not visible in the XRD pattern, we believe, on the basis of our previous experience with SBA-15, that the two-dimensional P6m hexagonal symmetry was kept. The spacing between the (100) planes,  $d_{100}$ , and the cell parameter,  $a_0$ , corresponding to the distance between the two pore centres, were 9.4 and 10.9 nm, respectively. The structural properties determined from the N<sub>2</sub> adsorption isotherms are shown in Figure 2. The isotherms displayed a type IV with H1 hysteresis characteristic of strongly organized mesoporous materials with a well-specified cylindrical pore morphology. The values for the BET surface area ( $S_{\text{BET}}$ ) and total pore volume ( $V_p$ ) are provided in Table 2, and the micropore volume ( $V_{\mu p}$ ) was 0.096 cm<sup>3</sup>/g. Figure 2b's inset shows the pore size distributions of the adsorption and desorption branches of the BJH method for a cylindrical pore model. The pore size was calculated using the BJH method from the adsorption branch, and the value was 7.0 nm. The mean wall thickness  $t$  was calculated taking into account the cell parameter, 10.9 nm, and the pore size, 7.0 nm, and a value of 3.8 nm was obtained.

**Table 1.** Surface functionalization experiments for silica SBA-15 with AEAPTS in scCO<sub>2</sub> modified with 10% mol methanol or ethanol at 323 K and approximately 12.5 MPa and in toluene at 323 K and atmospheric pressure. TGA measurements expressed as percentages of mass loss at the different temperature ranges, grafting density ( $\rho_m$ ) and surface coverage ( $\rho_s$ ).

<sup>1</sup> Sample	<sup>2</sup> $y \cdot 10^{-3}$	$p/\text{MPa}$	Time/Hour	TGA (% Mass)			<sup>3</sup> $\rho_{\text{m}}$ (mmol·g <sup>-1</sup> )	<sup>4</sup> $\rho_{\text{S}}$ (Molec·nm <sup>-2</sup> )
				301 to 383 K	383 to 598 K	598 to 1073 K		
scCO <sub>2</sub> modified with 10% mol methanol								
A1	0.6	12.5	2	1.2	4.3	7.8	0.8	0.8
A2	1.0	12.4	2	0.1	2.9	13.7	1.6	1.6
A3	1.7	12.7	3	2.5	3.0	17.4	2.1	2.1
scCO <sub>2</sub> modified with 10% mol ethanol								
A4	0.5	12.5	3	0.4	2.9	11.1	1.2	1.3
A5	1.0	12.5	2	2.5	2.8	11.2	1.2	1.3
A6	1.1	12.5	3			12.8	1.4	1.5
A7	1.8	12.5	3	2.1	2.9	17.3	2.1	2.1
Toluene								
C1	14.1	0.1	24	2.7	4.7	21.8	2.8	2.8
C2	6.0	0.1	24	1.9	3.7	19.4	2.4	2.4

<sup>1</sup> A1 to A3 were functionalized using scCO<sub>2</sub> modified with 10% methanol. A4 to A7 were functionalized using scCO<sub>2</sub> modified with 10% ethanol. C1 and C2 were functionalized in toluene.

<sup>2</sup> AEAPTS molar fraction ( $y_{\text{AEAPTS}}$ ). <sup>3</sup> Grafting density,  $\rho_m$ , calculated using TGA data in the range 598–1073 K and molar mass of the AEAPTS organic part ( $M = 101.2 \text{ g} \cdot \text{mol}^{-1}$ ) according to  $\rho_m = \frac{(\% \text{ mass loss})}{(100 - \% \text{ mass loss}) \cdot M}$ . <sup>4</sup> Surface coverage density,  $\rho_s$ , calculated using  $\rho_m$ , Avogadro number ( $N_A$ ) and the BET surface area of SBA-15 reported in Table 2 ( $S_{\text{BET}}$ ) according to  $\rho_s = \frac{N_A \cdot \rho_m}{S_{\text{BET}}}$ .



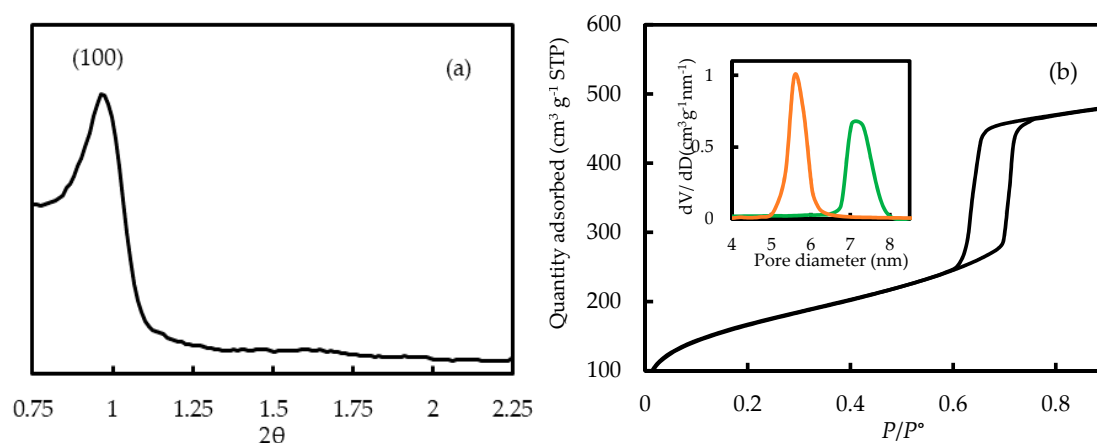


**Figure 2.** (a) Low-angle XRD patterns of silica SBA-15 support. (b)  $N_2$  adsorption–desorption isotherms for silica SBA-15. (b—inset) Barrett–Joyner–Halenda (BJH) pore size distribution curves from the adsorption branch (—) and the desorption branch (---) of the isotherm for silica SBA-15.

**Table 2.** Elemental analysis (EA) data expressed as mass percentages, and C/N molar ratios and  $N_2$  adsorption isotherms at 77 K; data showing the BET surface area ( $S_{BET}$ ), the total pore volume ( $V_p$ ) and the pore size for the bare silica SBA-15 and the diamine-functionalized samples.

<sup>1</sup> Sample	Elemental Analysis					$S_{BET}$ (m <sup>2</sup> ·g <sup>−1</sup> )	$V_p$ (cm <sup>3</sup> ·g <sup>−1</sup> )	Pore Size (nm)
	C/%	H/%	N/%	C, H, N/%	C: N			
SBA-15						590	0.81	7.1
				scCO <sub>2</sub> modified with 10% mol methanol				
A1	6.2	1.4	2.5	10	2.9	319	0.50	6.0
A2	9.1	2.0	3.8	15	2.8	141	0.22	5.4
A3	12.4	2.9	5.3	21	2.7	92	0.15	5.4
				scCO <sub>2</sub> modified with 10% mol ethanol				
A4	7.6	1.7	2.9	12	3.1	281	0.40	6.1
A5	8.2	1.8	3.5	14	2.7	267	0.42	5.9
A6	9.7	2.2	4.2	16	2.7	161	0.25	5.8
A7	12.5	2.4	4.5	19	3.2	103	0.15	5.4
				Toluene				
C1	16.8	3.4	7	27	2.8	11	0.02	-
C2	14.7	3.1	6.2	24	2.8	22	0.04	-

<sup>1</sup> A1 to A3 were functionalized using scCO<sub>2</sub> modified with 10% methanol. A4 to A7 were functionalized using scCO<sub>2</sub> modified with 10% ethanol. C1 and C2 were functionalized in toluene. Volume of micropore was 0.096 cm<sup>3</sup>/g for the bare silica SBA-15, and it was zero for all functionalized samples.

As may be seen in Table 1, the functionalization experiments were performed at 323 K and approximately 12.5 MPa, and a molar fraction range for AEAPTS between  $0.5 \cdot 10^{-3}$  and  $1.8 \cdot 10^{-3}$ . The different experimental conditions were selected taking into account the phase equilibrium data for mixtures of CO<sub>2</sub> and similar aminosilanes [18,23,24]. Sanchez-Vicente et al. [18] studied the phase behaviour of 3-aminopropyltrimethoxysilane (3APTS)/carbamate in scCO<sub>2</sub> modified with ca. 10% mol ethanol at temperatures of 313, 323 and 333 K in the 8.0–12.0 MPa pressure range and with  $1 \cdot 10^{-3}$  to  $4 \cdot 10^{-3}$  molar fractions of 3APTS, and they found that 3APTS/carbamate was soluble in a CO<sub>2</sub> + 10% ethanol mixture at 8.2, 9.8 and 12.0 MPa at 313, 323 and 333 K, respectively. It was also found that the solubility pressures were slightly higher than those reported for the CO<sub>2</sub> + 10% mol ethanol binary system. Table 3 shows the phase behaviour data for the CO<sub>2</sub> + 10% mol ethanol and CO<sub>2</sub> + 10% mol methanol binary systems. However, not only does the AEAPTS precursor have a higher molecular weight than 3APTS, but the diamine in the AEAPTS also shows a stronger affinity for CO<sub>2</sub> than the monoamine in 3APTS [31,32]. Therefore, full miscibility of AEAPTS/carbamate in a CO<sub>2</sub> + 10% mol ethanol or methanol mixture might be achieved at higher pressures than those reported for 3APTS. Overall, it was decided to perform the functionalization experiments with AEAPTS at 323 K

and a pressure much higher than that reported for the CO<sub>2</sub> + ethanol and CO<sub>2</sub> + methanol binary systems, 12.5 MPa. Under these conditions, the experiments might have been performed in a CO<sub>2</sub> expanded liquid. Here, we only explored the effect of the reaction time and silane concentration on the amine grafting on SBA-15, since we found in previous work that the influences of the pressure and temperature were insignificant [18,19]. For comparative purposes, SBA-15 was also functionalized in toluene at 323 K according to the conventional method (see Table 1).

Thermal gravimetric analysis (TGA) was used to determine the amount of amine bound to the SBA-15 silica as well as the thermal stability of the functionalized SBA-15. Figure 3 displays the mass loss versus temperature and its derivative versus temperatures for the two samples: Sample A7, functionalized in a CO<sub>2</sub> + 10% ethanol mixture, and Sample C2 modified in toluene. The TGA showed relatively high mass losses due to the diamine decomposition. Three characteristic weight losses were identified from the first derivative of the weight loss (see Figure 3b) for all the functionalized samples at the following temperature intervals: 301 to 383 K, 383 to 598 K, and 598 to 1073 K. Similar temperature intervals were found in the literature for SBA-15 grafted with AEPTS [29,33]. The section under 383 K was related to desorption of residual alcohol, carbon dioxide or water physically adsorbed. The mass reduction from 383 to 598 K may be related to AEPTS molecules physisorbed and hydrogen-bonded silanol on the support and represents an amount of less than 5 percent of the total mass loss, indicating that most of the precursor was covalently attached to the silica surface, as can be seen in Table 1. The most considerable mass loss was between ca. 598 and 1073 K due to the degradation of the firmly attached amine compounds by the breakup of the Si–C and the C–C bonds. The maximum rate of the weight loss calculated by the derivation of the mass loss versus time occurred in the range of 700 to 720 K. These results indicated that the prepared amino-silica SBA-15 was extremely stable until about 598 K, so they can be used in the temperature swing adsorption process. The grafting density ( $\rho_m$ ) of the functionalized silica in millimoles of N-propylethylenediamine per gram of silica was determined using the percentage of mass loss from 598 to 1073 K and the molecular mass of N-propylethylenediamine, 101.2 g·mol<sup>−1</sup>. The surface coverage density,  $\rho_s$ , of the functionalized samples, the number of N-propylethylenediamine molecules per square nanometre, was estimated by dividing the  $\rho_m$  by the surface area of the bare silica SBA-15 and multiplying by the Avogadro number. The values for both magnitudes,  $\rho_m$  and  $\rho_s$ , are reported in Table 1 for all the samples studied in this paper; these values were obtained by TGA following the same procedure described for Samples A7 and C1.

**Table 3.** Phase behaviour for CO<sub>2</sub> + methanol and CO<sub>2</sub> + ethanol binary mixtures. Bp is the bubble point; Dp, the dew point; and  $x$ , the molar fraction of ethanol or methanol in the mixture.

System	$x$	$T/K$	$p/MPa$	Transition	Reference
CO <sub>2</sub> + methanol	0.106	313	8.1	Bp	[34]
	0.106	323	9.6	Bp	[34]
	0.106	333	11.1	Dp	[34]
CO <sub>2</sub> + ethanol	0.105	313	7.9	Bp	[35]
	0.101	323	9.1	Bp	[36]
	0.098	333	10.5	Dp	[35]



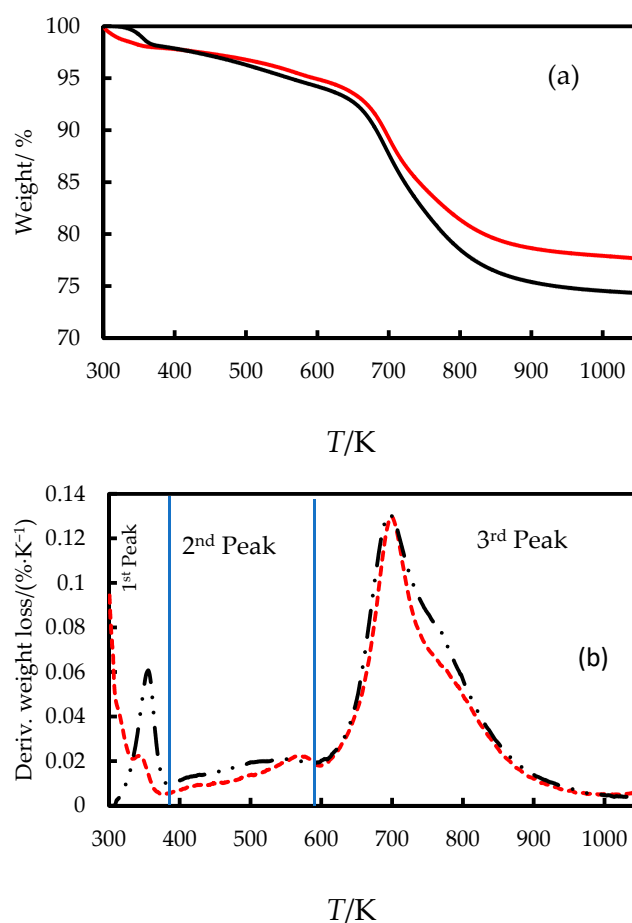


**Figure 3.** (a) Thermal gravimetric analysis (TGA) and (b) the first derivative of TGA curves for diamine-silica SBA-15 functionalized in  $\text{scCO}_2$  modified with 10% mol ethanol, Sample A7 (—, —), and in toluene, Sample C2 (—, —).

The elemental analysis (EA) of the samples was also performed to corroborate the total weight loss measured by TGA and understand the chemical formula of the diamine grafted to the surface of the silica SBA-15. Table 2 provides the results of the EA. The total mass percentages (C, H and N) determined from the elemental analysis on the functionalized samples agreed with the mass percentage loss determined by TGA. The theoretical C/N molar ratio that corresponds to the N-propylethylenediamine is 2.5. The experimental C/N molar ratio was higher than 2.8 for all the studied samples (see Table 2). The slightly higher proportion of the molar C/N ratio may be attributed to the incomplete hydrolysis of the AEAPTS and/or the existence of residual alcohol as well as the presence of AEAPTS molecules physisorbed on the silica. Moreover, Zeng et al. identified carbon dioxide by mass spectrometry during the first mass loss event from the TGA, and they believed that  $\text{CO}_2$  was adsorbed by the sample from ambient air [29]. Therefore, the higher C/N ratio could also be due to carbon dioxide that was adsorbed from the air.

The  $\text{N}_2$ -adsorption/desorption isotherms of the functionalized samples were also evaluated to provide more knowledge on the distribution of amine groups across silica SBA-15, and they are shown in Figure 4. The  $S_{\text{BET}}$  and  $V_p$  values are provided in Table 2. The silica functionalized using  $\text{scCO}_2$  modified with alcohol retained the type IVa isotherm with the H1 hysteresis loop found in the bare SBA-15 silica [37]. However, the isotherms for the samples functionalized using the traditional method were type II, which is representative for non-porous material. This indicated that the pore was filled with AEAPTS. Surprisingly, the volume of the micropore was zero for all the modified materials, suggesting that the micropores in the bare silica SBA-15 had been filled or blocked after the grafting process.

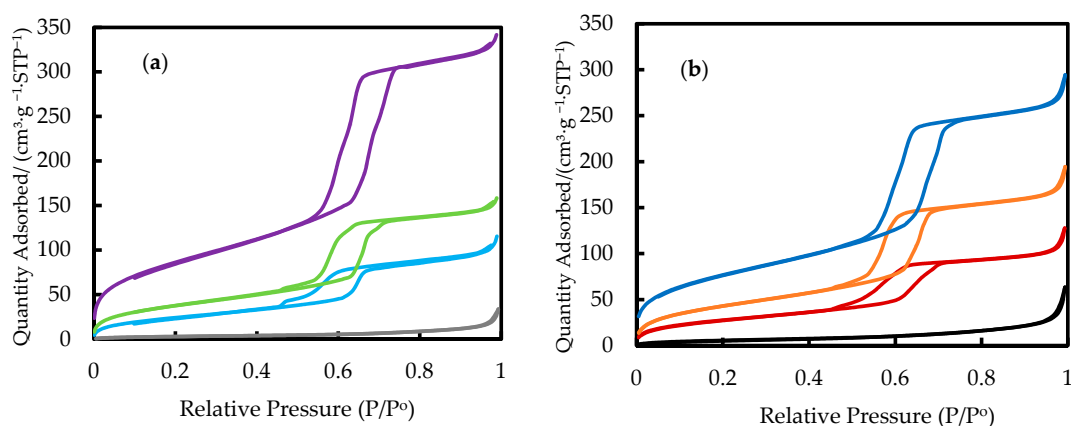


**Figure 4.**  $N_2$  adsorption–desorption isotherms for amine-functionalized silica SBA-15: (a) using  $scCO_2$  modified with 10% methanol; (—) Sample A1, (—) Sample A2 and (—) Sample A3; and using toluene, Sample C1 (—), and (b) using  $scCO_2$  modified with 10% ethanol; (—) Sample A4, (—) Sample A6 and (—) Sample A7—and using toluene, Sample C2 (—).

Figure 5 shows the BJH pore size distribution curves calculated from the adsorption and desorption branches of the isotherms for the functionalized materials. Table 2 shows the maximum pore size determined using the adsorption branch. The BJH distribution measured from the desorption branch of the isotherm revealed a new peak of 3.2 nm, which depends on the adsorbate used, in this case,  $N_2$ , and that does not imply the existence of the pore size in this range [38].

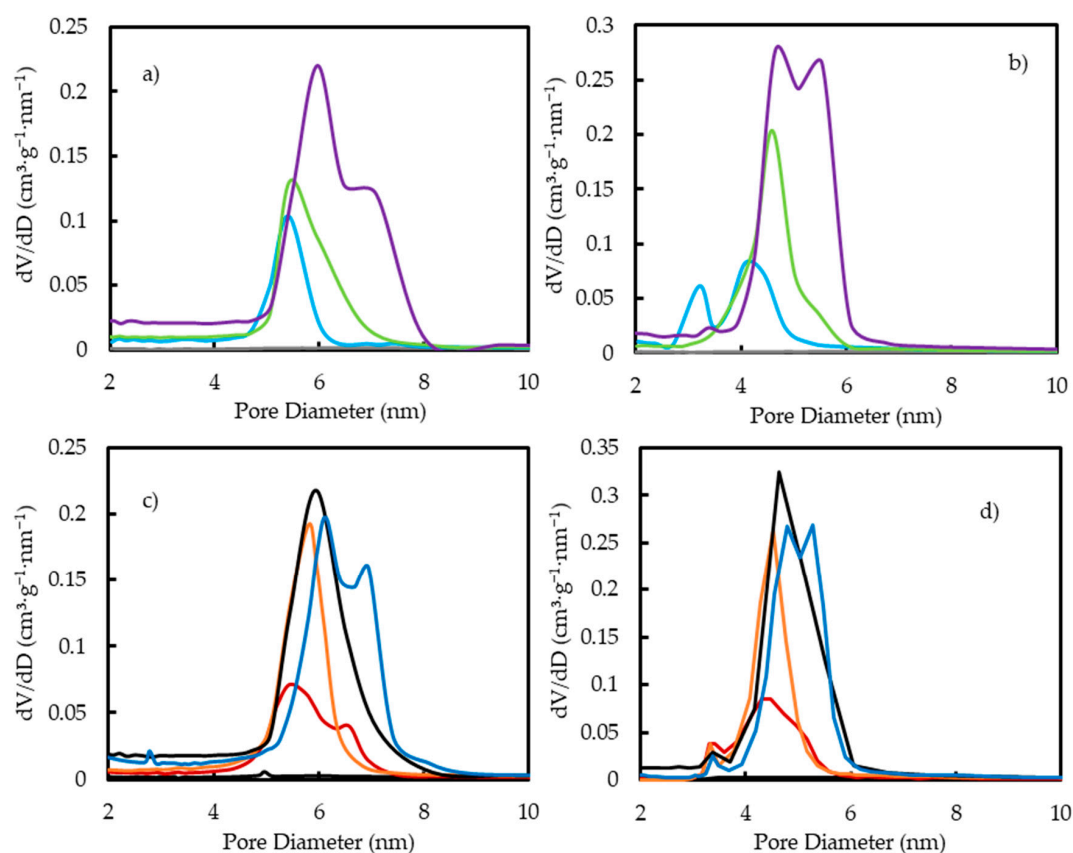


**Figure 5.** BJH pore size distribution curves from the adsorption branch (a,c) and the desorption branch (b,d) of the isotherm for functionalized silica SBA-15 using (a,b)  $scCO_2$  modified with methanol; (—) Sample A1, (—) Sample A2 and (—) Sample A3 and (c,d) using  $scCO_2$  modified with 10% ethanol: (—) Sample A4, (—) Sample A5, (—) Sample A6 and (—) Sample A7.

### 3.2. Excess Carbon Dioxide Adsorption

The amine loading density ( $\rho_N$ ) of functionalized silica SBA-15, which includes the quantities of impregnated and grafted amine, is an essential parameter for evaluating the CO<sub>2</sub> adsorption capacity. Table 4 shows the amine loading density for the obtained samples calculated using the mass percentage of nitrogen from the elemental analysis (see Table 2). Samples functionalized in scCO<sub>2</sub> modified with alcohol exhibited amine loads that ranged from 1.3 to 3.8 mmol N·g<sup>-1</sup>, which are close to those published in the literature using toluene as a solvent [32,39].

**Table 4.** Amine loading density ( $\rho_N$ ) of functionalized silica SBA-15 calculated from the nitrogen mass percent obtained from the elemental analysis shown in Table 2. Excess CO<sub>2</sub> adsorption capacities at several temperatures and atmospheric pressure. Amine efficiency at 298 and 333 K.

Sample Name <sup>1</sup>	$\rho_N$ (mmol N·g <sup>-1</sup> )	Excess CO <sub>2</sub> Adsorption (mmol·g <sup>-1</sup> )								Amine Efficiency (mol CO <sub>2</sub> ·mol <sup>-1</sup> N)	
		T/K								T/K	
		298	313	333	353	373	393	413	433	298	333
SBA-15	0.0	0.60	0.40	0.23	0.14	0.08	0.04	0.01	0.00		
<b>scCO<sub>2</sub> modified with 10% mol methanol</b>											
A1	1.8	0.74	0.61	0.45	0.33	0.22	0.13	0.15	0.12	0.41	0.25
A2	2.7	0.89	0.79	0.66	0.53	0.36	0.18	0.18	0.12	0.33	0.24
A3	3.8	0.75	0.77	0.86	0.89	0.77	0.48	0.35	0.26	0.20	0.23
<b>scCO<sub>2</sub> modified with 10% mol ethanol</b>											
A4	2.1	0.79	0.70	0.64	0.56	0.43	0.30	0.20	0.24	0.38	0.31
A5	2.5	0.84	0.73	0.57	0.42	0.28	0.13	0.15	0.10	0.34	0.23
A6	3.0	0.90	0.86	0.78	0.66	0.48	0.26	0.24	0.17	0.30	0.26
A7	3.2	0.61	0.64	0.69	0.64	0.50	0.31	0.19	0.16	0.19	0.22
<b>Toluene</b>											
C1	5.0	0.15	0.19	0.52	1.08	1.31	0.93	0.43	0.37	0.03	0.10
C2	4.4	0.31	0.39	0.79	1.12	1.03	0.66	0.33	0.28	0.07	0.18

<sup>1</sup> A1 to A3 were functionalized using scCO<sub>2</sub> modified with 10% methanol. A4 to A7 were functionalized using scCO<sub>2</sub> modified with 10% ethanol. C1 and C2 were functionalized in toluene.

The excess CO<sub>2</sub> adsorption capacities of the amine-functionalized samples and bare silica at atmospheric pressure and various temperatures are shown in Table 4 and Figure 6. The adsorption capacity was defined as the ratio of adsorbed CO<sub>2</sub> mol and sample mass (mmol CO<sub>2</sub>·g<sup>−1</sup> sample). The amine efficiency was calculated by dividing the amount of CO<sub>2</sub> adsorbed and the amine loading quantity (mol CO<sub>2</sub>·mol N<sup>−1</sup>). This quantity is a useful instrument for comparing adsorbents. Table 3 reports the amine efficiencies at 298 and 333 K, as typical temperatures for direct air capture and post-combustion capture, respectively.

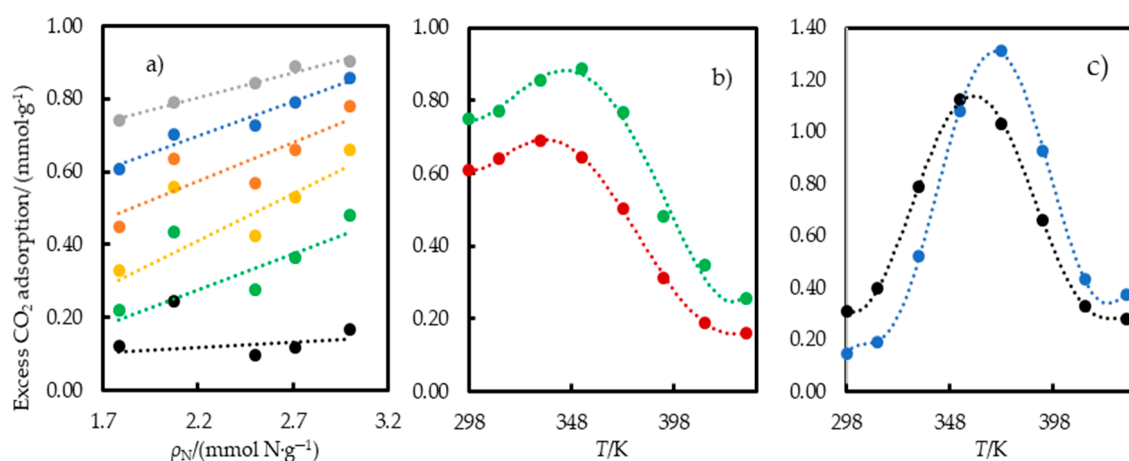


**Figure 6.** Excess CO<sub>2</sub> adsorption capacity for several amine loadings;  $\rho_N$  at eight temperatures for samples obtained by scCO<sub>2</sub> method (a,b) and toluene method (c). (a) Amine loading up to 3 mmol N·g<sup>−1</sup> at temperatures of •, 298; •, 313; •, 333; •, 353; •, 373; and •, 433 K. (b) Amine loading: •, 3.8, and, •, 3.2 mmol N·g<sup>−1</sup>. (c) Amine loading: •, 5.0, and •, 4.4 mmol N·g<sup>−1</sup>.

## 4. Discussion

### 4.1. Functionalization of Silica SBA-15 with AEAPTS

A possible simplified scheme illustrating the functionalization of silica SBA-15 with AEAPTS in scCO<sub>2</sub> modified with 10% mol methanol or ethanol is presented in Figure 7. Firstly, CO<sub>2</sub> reacts with the secondary and primary amines of AEAPTS and produces insoluble carbamate salts through the zwitterionic mechanism [40,41]. The ammonium carbamate formation is a very fast equilibrium reaction, so it occurs before the silanization reaction [42]. In more detail, the lone pair of electrons on the nitrogen atom of the primary amine attacks the carbon atom of CO<sub>2</sub>, forming a zwitterionic compound, and then, one of the hydrogen atoms from the primary amine moves to the oxygen of CO<sub>2</sub>, producing carbamic acid that is difficult to detect. Carbamic acid is deprotonated by the second amine group present in the amino silane molecule, providing an intramolecular cyclic ammonium carbamate silane: (2-((3-(trimethoxysilyl)propyl)ammonio)ethyl)carbamate, TSPAEC-carbamate [40]. Since the CO<sub>2</sub> is in excess in the reaction medium, the equilibrium reaction is displaced to the right, toward TSPAEC-carbamate production. However, both compounds are in the reaction medium. Secondly, the water hydrolyses the intramolecular ammonium carbamate silane to an ammonium carbamate silanol [43]. In our experiments, the water content was about 0.2% mol, and it was either adsorbed on the surface of the silica or dissolved in the solvent. Finally, the ammonium carbamate silanol condenses with adjacent molecules or silanol groups of the surface to form siloxane bonds (Si–O–Si) and water. It could be possible that condensation might begin before the completion of the hydrolysis, generating siloxane bonds (Si–O–Si) plus methanol. The silanization of trialkoxysilanes could produce multiple surface structures such as vertical polymerization, horizontal polymerization and covalent attachment (the only structure shown in Figure 7) [44,45]. Once the silanization reaction was completed, the amine-functionalized silica SBA-15 was obtained by removing the CO<sub>2</sub> from the ammonium carbamate salt through heating up the sample.

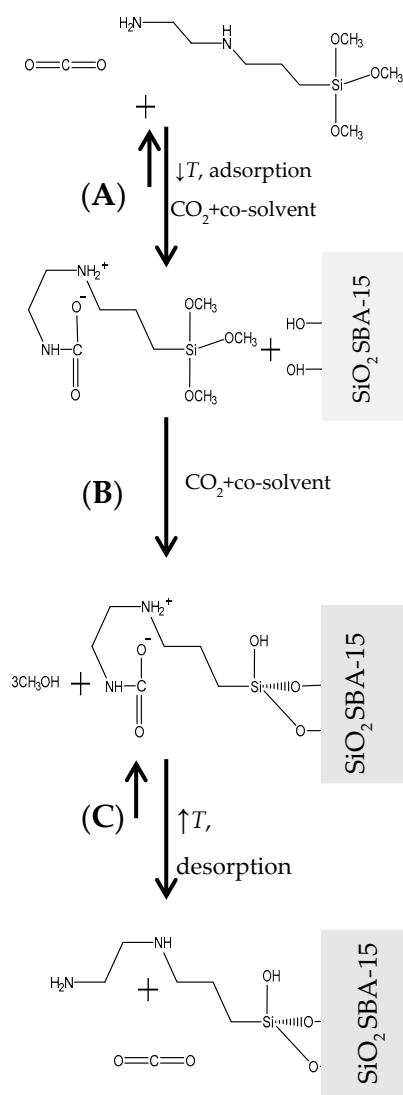


**Figure 7.** Possible simplified mechanism for the reaction between AEAPTS and silica SBA-15 in  $\text{scCO}_2$  plus 10% mol methanol or ethanol mixtures. (A) 2-((3-(trimethoxysilyl)propyl)ammonio)ethyl)carbamate (TSPAEC-carbamate) formation, (B) silanization reaction and (C)  $\text{CO}_2$  desorption and formation of the diamine-functionalized silica SBA-15.

The impact of the reaction time and molar fraction of the AEAPTS on the amine attaching to SBA-15 when using the  $\text{scCO}_2$  method is discussed here. Two experiments were performed in  $\text{scCO}_2$  modified with 10% ethanol with two reaction times: 2 and 3 h (Samples A5 and A6 in Tables 1 and 2). As can be seen from Table 1, the grafting density increased slightly as the reaction time increased. Analogously, the  $S_{\text{BET}}$  and  $V_p$  of the functionalized silica samples decreased with time. However, the experimental C/N molar ratio was the same for both experiments. The increase in the reaction time also led to a rise in the amount of amine attached to the silica with respect to the amine physisorbed in the silica (see Tables 1 and 2). It seems that as the reaction time increased, more amino-silane penetrated and attached inside the pore, producing much lower  $S_{\text{BET}}$  and  $V_p$ . This indicates that an increase in reaction time could promote the infiltration of the precursor into the silica pores. Similar results were obtained in our previous studies for the surface modification of silica SBA-15 with DMAPTS and TMS in  $\text{scCO}_2$  [19,46]. The effect of the AEAPTS molar fraction on the grafting density was also studied at 12.5 MPa and 313 K for both cosolvents, methanol and ethanol. As can be seen from Table 1, the grafting and surface coverage densities increased gradually as the AEAPTS molar fraction increased. These findings demonstrated that it was possible to control the diamino grafting density on



silica SBA-15 by choosing the concentration of AEAPTS for scCO<sub>2</sub> modification. A maximum value of 2.1 mmol·g<sup>−1</sup> was reached for a molar fraction of AEAPTS of 1.8·10<sup>−3</sup>. López-Aranguren et al. [23] reported lower grafting densities (ca. 0.5 mmol/g<sup>−1</sup>) for the functionalization of mesoporous silica MCM-41 and silica gel with AEAPTS at 9.0 MPa and 408 K using scCO<sub>2</sub>. This result could be attributed to the low solubility of AEAPTS in the CO<sub>2</sub> phase. Therefore, our proposed functionalization route can be considered more efficient than the one suggested in the literature.

For diamine-silica SBA-15 prepared in scCO<sub>2</sub>, the surface area, pore volume and pore size decreased gradually as the amount of amine loading into the silica increased, as can be seen in Table 2. Figure 4 shows that the volume of gas adsorbed steadily decreased and the isotherms shifted downwards as the diamine content rose. The BJH pore distribution also shifted regularly to lower values as the amount of amine in SBA-15 increased, as can be seen in Figure 5. The functionalized samples with larger amine loads (A3 and A7) show  $S_{\text{BET}} \leq 100 \text{ m}^2\cdot\text{g}^{-1}$  and  $V_p < 0.25 \text{ cm}^3 \text{ g}^{-1}$ , indicating that a closely packed amino layer could have been formed inside the pores in these samples. A theoretical length of ca. 1.0 nm was estimated using the ChemDraw 18.2 software for NH<sub>2</sub>–(CH<sub>2</sub>)<sub>2</sub>–NH–(CH<sub>2</sub>)<sub>3</sub>–Si–. A closely packed amino monolayer inside the pores would reduce the pore size to double the length of the organic chain, so the pore size should be ca. 5.1 nm. The pore sizes obtained using the scCO<sub>2</sub> method were close to theoretical sizes for Samples A2, A3 and A7, indicating that a compact monolayer could have been achieved. On the other hand, similar amino-grafting densities were obtained for both cosolvents, methanol and ethanol, as is shown in Table 1. Therefore, the silica SBA-15 can be functionalized with diamine using either cosolvent, but ethanol is less toxic than methanol and can be easily produced in fermentation processes.

For the studies that were performed utilizing the traditional toluene method, described in Table 1, the amount of amine grafting was found to be consistent with the values previously reported in the literature [29,32,33,39,47]. The samples obtained by the traditional method showed minimal pore volumes and surface areas and were non-porous. These results indicated the filling of the pore with diamino compounds, presumably due to the vertical polymeric deposition. Comparing both methods, in this work, the functionalization experiments for the scCO<sub>2</sub> modified with alcohol were faster (3 h) than those for toluene (24 h). In general, long reaction times of 24 h were required to obtain a significant amount of loading with the traditional method [17]. This may be due to the superior transport properties of the CO<sub>2</sub> + alcohol medium in comparison to toluene [26] as well as the fact that CO<sub>2</sub> could produce bicarbonates/carbonates with water impurities that can catalyse the hydrolysis and condensation of the diaminosilane [48]. Furthermore, the high pressure in the scCO<sub>2</sub> method could accelerate the reaction, pushing the reaction equilibrium towards the condensed form, since the silanization reaction has a negative volume of activation and reaction [20].

On the other hand, the  $\rho_m$  values were slightly lower in the samples obtained in the CO<sub>2</sub> + alcohol medium than in those obtained in toluene. This could be due to the AEAPTS concentrations in the solution that were six times lower in the modified scCO<sub>2</sub> than in toluene, promoting vertical polymerization. As can be seen in Table 2, the  $S_{\text{BET}}$  and  $V_p$  values of the conventional method samples were much lower than those found in the samples using the scCO<sub>2</sub> method. As was mentioned before, the samples obtained in toluene did not exhibit mesopores, while the SBA-15 porosity was preserved in the samples obtained in scCO<sub>2</sub>. The main distinction between the scCO<sub>2</sub> and the toluene methods was that the silane agents might be different. The silane agent was possibly TSPAЕ-carbamate (intramolecular carbamate) in the scCO<sub>2</sub> method, while AEAPTS was the precursor in the toluene process. The Connolly solvent-excluded volumes for the TSPAЕ-carbamate and AEAPTS molecules were estimated using the ChemDraw 18.2 software. The values were 171.2 and 199.8 Å<sup>3</sup> for the AEAPTS and TSPAЕ-carbamate molecules, respectively. The lower grafting density found in the samples using the scCO<sub>2</sub> method might be explained by the struggling of the bulky TSPAЕ-carbamate to diffuse inside the pores compared to the AEAPTS. Nevertheless, different silane agents can interact differently with their solvents and surfaces, so both methods could produce diverse surface structures and grafting densities [49].

Comparing the samples modified using the 3-aminopropyl precursor reported in our previous work [18] and the sample modified using the 3-(2-aminoethylamino)propyl precursor presented here, it was observed that for the same grafting density, the decrease in surface area and pore volume with respect to the bare SiO<sub>2</sub> material was higher for the sample functionalized with 3-(2-aminoethylamino)propyl, most likely due to the larger size of the organic moiety. This can be seen clearly for samples functionalized in toluene.

#### 4.2. Excess CO<sub>2</sub> Adsorption

CO<sub>2</sub> physical adsorption is the primary mechanism that contributes to the CO<sub>2</sub> adsorption capacities on bare silica SBA-15. For functionalized silica samples, the key mechanism for the low-pressure adsorption of CO<sub>2</sub> is the chemical reaction between the CO<sub>2</sub> and the primary and secondary amine groups, especially for those samples with high amine loading. Mafrá et al. studied the structure of chemisorbed CO<sub>2</sub> species in amine-functionalized silica SBA-15 by solid-state NMR and computer modelling, and they identified at least three chemisorbed CO<sub>2</sub> species (essentially carbamic acid and alkylammonium carbamate-like ion pairs) [31,32]. According to these authors, the diamine samples showed strong interaction with CO<sub>2</sub> due to chemisorption, but some physisorbed CO<sub>2</sub> is in equilibrium with chemisorbed CO<sub>2</sub> even at low pressure. In this work, it was assumed that the CO<sub>2</sub> adsorption capacity was due mainly to CO<sub>2</sub> chemisorption, though some CO<sub>2</sub> was also physically adsorbed on any bare silica left. In general, two main factors affect the CO<sub>2</sub> adsorption capacities: amine loading and the available pore volumes of the material after functionalization. The remaining pore volume should be sufficiently large to allow the diffusion of CO<sub>2</sub> through the pore and thus it reaching the amine adsorption sites.

For samples with  $\rho_N \leq 3 \text{ mmol N} \cdot \text{g}^{-1}$ , the excess CO<sub>2</sub> adsorption capacity increased almost linearly with increasing amine loading at all temperatures; see Table 4 and Figure 6a. Furthermore, for these samples, the excess CO<sub>2</sub> adsorption capacity decreased as the temperature increased, since both the adsorption heat and change in entropy are negative for the adsorption process. At 433 K, the remaining CO<sub>2</sub> in all the samples was about  $0.1 \text{ mmol CO}_2 \cdot \text{g}^{-1}$ , except for Sample A4. It seems that in sample A4, physisorbed silane might have moved and plugged some of the pores during the CO<sub>2</sub> desorption process. The maximum excess CO<sub>2</sub> adsorption capacity was  $0.90 \text{ mmol CO}_2 \cdot \text{g}^{-1}$  at 298 K, obtained for Sample A6. Moreover, the amine efficiency for these samples ranged from 0.4 to 0.3 mol CO<sub>2</sub> · mol<sup>−1</sup> N at 298 K, as can be seen in Table 4. The amine efficiency decreased as the temperature increased as a result of excess CO<sub>2</sub> adsorption reduction. At 333 K, the amine efficiencies were about 0.25 mol CO<sub>2</sub> · mol<sup>−1</sup> N. These findings are in agreement with the mechanism of carbamate formation. However, as there is always a fraction of CO<sub>2</sub> that is physisorbed on the substrate, the amine efficiency value might be slightly lower.

For samples with  $\rho_N > 3 \text{ mmol N} \cdot \text{g}^{-1}$ , the excess CO<sub>2</sub> adsorption capacity increased with increasing temperature until a maximum was reached, after which it decreased monotonically (see Figure 6b,c). The maximum excess CO<sub>2</sub> adsorption capacity was  $1.31 \text{ mmol CO}_2 \cdot \text{g}^{-1}$  at 373 K, obtained for Sample C1. However, the amine efficiency for these samples ranged from 0.2 to 0.03 mol CO<sub>2</sub> · mol<sup>−1</sup> N at 298 K and from 0.23 to 0.1 mol CO<sub>2</sub> · mol<sup>−1</sup> N at 333 K, as can be seen in Table 4. This suggested that many of the amine sites were inaccessible to the CO<sub>2</sub>. These samples showed high amine loading, but the pore volume was tiny after the functionalization, about  $0.15 \text{ cm}^3 \cdot \text{g}^{-1}$  for Samples A3 and A7 and  $0.02 \text{ cm}^3 \cdot \text{g}^{-1}$  for Samples C1 and C2. Therefore, the diffusion of CO<sub>2</sub> into the diamino-SBA-15 pore would be limited due to the dense diamino layer and carbamate formation that could produce the blockage of the pores. For these adsorbents, an increase in the operating temperature caused an increase in CO<sub>2</sub> capacity because the temperature enhanced the CO<sub>2</sub> diffusion and accessibility of the amino sites.

As can be seen in Table 4, the excess CO<sub>2</sub> adsorption capacity in amine-silica SBA-15 was higher than that of bare SBA-15, except at 298 and 313 K for Samples C1 and C2 due to the poor diffusion of CO<sub>2</sub> to reach the amine sites in these samples. Comparing the samples obtained by both methods,

the excess CO<sub>2</sub> adsorption values at  $T < 333$  K were lower for the samples prepared in the toluene medium than for those obtained in the scCO<sub>2</sub> + alcohol medium. Furthermore, the amine efficiency values of the samples obtained with the scCO<sub>2</sub> method were higher than those found for the samples prepared using the conventional method, particularly at 298 K. The samples obtained in toluene, as stated earlier, lacked pores. At the same time, the porosity of SBA-15 was retained in the scCO<sub>2</sub> samples, allowing the diffusion of CO<sub>2</sub> through the pore and it reaching the amine adsorption sites. Table 5 shows the CO<sub>2</sub> adsorption capacities and amine efficiencies reported for similar materials and under similar condition by other authors. The values of these properties for the materials obtained here were comparable to or better than those reported in the literature. Comparing the excess CO<sub>2</sub> adsorption capacities and amine efficiencies for the diamine-silica SBA-15 prepared in this work and the primary amine-silica SBA-15 synthesized in our previous work [18], as presented in Table 5, it was observed that the CO<sub>2</sub> capacities and amine efficiencies for similar amine loadings were higher for the sample functionalized with a primary amine. These results might suggest that an intramolecular carbamate salt was not formed during the CO<sub>2</sub> adsorption because the compact layer of amine inside the silica pore might hinder the bending of a long organic chain that is needed to produce the intramolecular carbamate; see Figure 7. This means that two amine groups from different molecules were required to react with a single CO<sub>2</sub> molecule in the diamine-silica SBA-15, in the same way as in primary amine-silica. Therefore, comparing the grafting density,  $\rho_m$ , for both samples, diamine-silica SBA-15 shows values lower than those of the primary amine-silica SBA-15 (2–2.7 mmol/g<sup>−1</sup>), and that would explain the higher CO<sub>2</sub> adsorption for the primary amine. Hiyoshi et al. reported similar results to us [39,50]. The validation of these observations will entail studies similar to those performed by Mafra and coworkers [31,32] using solid-state nuclear magnetic resonance.

**Table 5.** Amine loading density ( $\rho_N$ ), CO<sub>2</sub> adsorption capacities and amine efficiency reported in the literature.

Support/Agent	$\rho_N$ /(mmol N·g <sup>−1</sup> )	Adsorption Condition		CO <sub>2</sub> Adsorption (mmol·g <sup>−1</sup> )	Amine Efficiency (mol CO <sub>2</sub> ·mol <sup>−1</sup> N)	Ref.
		$p_{CO_2}$ /kPa	$T$ /K			
SBA-15/AEAPTS	3.9	100	298	1.40	0.38	[32]
SBA-16/AEAPTS	7.7	100	300	0.80	0.10	[33]
SBA-16/AEAPTS	2.1–2.6	15	333	0.30–0.60	0.14–0.29	[47]
SBA-15/AEAPTS	4.2	15	333	0.87	0.21	[50]
SBA-15/AEAPTS	4.6	100	292	1.95	0.42	[29]
SBA-15/AEAPTS	2.3	15	333	0.26	0.11	[39]
SBA-15/AEAPTS	3.8	15	333	0.87	0.23	[39]
SBA-15/3APTS <sup>1</sup>	2.5–3.0	100	298	1.00–1.46	0.49–0.40	[18]

<sup>1</sup> 3APTS; 3-aminopropyltriethoxysilane.

Although the long-term stability of the materials obtained with the supercritical method has not been studied, the change in their properties when cycling experiments are performed should be very similar to that reported for the material synthesized in toluene. The stability of this diamine-silica over the cyclic adsorption/desorption of CO<sub>2</sub> was investigated by Khatri et al. [51] and Zheng et al. [29]. They observed that covalently attached diamino-silica was fully regenerable and stable upon cycling. Nonetheless, the obtained diamine-sorbent is in the early stages of development, and several challenges need to be resolved before it can be commercially applied. For instance, investigation of the performance of the amine sorbents under real gas conditions using different reactor configurations is needed [52,53].

## 5. Conclusions

It has been proved that the surface of silica SBA-15 can be functionalized with AEAPTS in scCO<sub>2</sub> modified with 10% mol methanol or ethanol at 12.5 MPa and 323 K. In general, the diamine-grafting density increased steadily as the AEAPTS concentration in the CO<sub>2</sub> + alcohol mixtures rose until about

2.1 mmol/g<sup>-1</sup>. In the same way, as the amine loading increased on the silica surface, the pore size,  $S_{\text{BET}}$  and  $V_p$  values decreased progressively. Comparing the scCO<sub>2</sub> method and the traditional process using toluene, the SBA-15 porosity was preserved after functionalization in the samples obtained with the scCO<sub>2</sub> method, but this was not the case for the materials grafted in toluene. However, the diamine-grafting densities obtained for the scCO<sub>2</sub> method were lower than those obtained with the toluene method. The main difference between the two methods was that the silane precursors might be different. The silane agent was probably TSPAЕ-carbamate (intramolecular carbamate) in the scCO<sub>2</sub> process, while AEAPTS was the precursor in the toluene method.

The excess CO<sub>2</sub> adsorption capacities for diamine-functionalized materials were measured at atmospheric pressure. For samples with amine loading lower than or equal to 3 mmol N·g<sup>-1</sup>, the CO<sub>2</sub> adsorption increased with an increase in amine loads and decreased with temperature. The materials with amine loading higher than 3 mmol N·g<sup>-1</sup> seemed to have hindering effects on the CO<sub>2</sub> diffusion through the pores of the silica, so an increase in operating temperature caused an increase in CO<sub>2</sub> capacity. The maximum amine efficiency was 0.4 mol CO<sub>2</sub>·mol<sup>-1</sup> N at 298 K. For similar amine loadings, the CO<sub>2</sub> capacities and amine efficiencies found for the sample functionalized with 3APTS in our previous work were higher than those of the diamine-grafted sample. This may indicate that no intramolecular carbamate salt was formed during CO<sub>2</sub> adsorption for the diamine-silica SBA-15. The CO<sub>2</sub> adsorption capacities and amine efficiencies presented here for the diamine-silica prepared using the scCO<sub>2</sub> method were comparable to or better than those reported for diamine-silica obtained using the traditional process by other authors. Therefore, scCO<sub>2</sub> plus alcohol mixtures can be used as a sustainable alternative to the organic solvent to functionalize silica SBA-15 with diaminosilanes, obtaining adsorbents with great potential for CO<sub>2</sub> capture applications.

**Author Contributions:** Conceptualization, Y.S.-V.; methodology, Y.S.-V. and L.S.; validation, Y.S.-V., L.S. and A.C.; formal analysis, Y.S.-V.; investigation, Y.S.-V. and L.S.; resources, L.S., C.P. and A.C.; writing—original draft preparation, Y.S.-V.; writing—review and editing, Y.S.-V., L.S., A.C. and C.P.; project administration, C.P.; funding acquisition, A.C. and C.P. All authors have read and agreed to the published version of the manuscript.

**Funding:** This research was funded by Spanish Ministry of Science and Innovation, grant number CTQ2010-16940. Y.S.V. was funded by a postdoctoral grant (PICATA program).

**Acknowledgments:** Y.S.-V. thanks the Campus de Excelencia Internacional Moncloa at UCM for their support through a postdoctoral grant (PICATA program). We are grateful to M.J. Torralvo and C.E. Snape and to J. Morère at UCM for their advice and assistance.

**Conflicts of Interest:** The authors declare no conflict of interest. The funders had no role in the design of the study; in the collection, analyses or interpretation of data; in the writing of the manuscript; or in the decision to publish the results.

## References

1. OECD. *Towards Green Growth?* OECD Publishing: Paris, France, 2015. [[CrossRef](#)]
2. United Nations. *COP21 Paris Agreement*; United Nations Framework Convention on Climate Change: Paris, France, 2016.
3. Bui, M.; Adjiman, C.S.; Bardow, A.; Anthony, E.J.; Boston, A.; Brown, S.; Fennell, P.S.; Fuss, S.; Galindo, A.; Hackett, L.A.; et al. Carbon capture and storage (CCS): The way forward. *Energy Environ. Sci.* **2018**, *11*, 1062–1176. [[CrossRef](#)]
4. Boot-Handford, M.E.; Abanades, J.C.; Anthony, E.J.; Blunt, M.J.; Brandani, S.; Mac Dowell, N.; Fernández, J.R.; Ferrari, M.-C.; Gross, R.; Hallett, J.P.; et al. Carbon capture and storage update. *Energy Environ. Sci.* **2014**, *7*, 130–189. [[CrossRef](#)]
5. Choi, S.; Drese, J.H.; Jones, C.W. Adsorbent Materials for Carbon Dioxide Capture from Large Anthropogenic Point Sources. *ChemSusChem* **2009**, *2*, 796–854. [[CrossRef](#)]
6. Goel, C.; Kaur, H.; Bhunia, H.; Bajpai, P.K. Carbon dioxide adsorption on nitrogen enriched carbon adsorbents: Experimental, kinetics, isothermal and thermodynamic studies. *J. CO<sub>2</sub> Util.* **2016**, *16*, 50–63. [[CrossRef](#)]

7. Rogacka, J.; Seremak, A.; Luna-Triguero, A.; Formalik, F.; Matito-Martos, I.; Firlej, L.; Calero, S.; Kuchta, B. High-throughput screening of metal – Organic frameworks for CO<sub>2</sub> and CH<sub>4</sub> separation in the presence of water. *Chem. Eng. J.* **2021**, *403*, 126392. [[CrossRef](#)]
8. Dou, B.; Wang, C.; Song, Y.; Chen, H.; Jiang, B.; Yang, M.; Xu, Y. Solid sorbents for in-situ CO<sub>2</sub> removal during sorption-enhanced steam reforming process: A review. *Renew. Sust. Energ. Rev.* **2016**, *53*, 536–546. [[CrossRef](#)]
9. Hu, X.; Liu, L.; Luo, X.; Xiao, G.; Shiko, E.; Zhang, R.; Fan, X.; Zhou, Y.; Liu, Y.; Zeng, Z.; et al. A review of N-functionalized solid adsorbents for post-combustion CO<sub>2</sub> capture. *Appl. Energy* **2020**, *260*, 114244. [[CrossRef](#)]
10. Zhang, S.; Chen, C.; Ahn, W.-S. Recent progress on CO<sub>2</sub> capture using amine-functionalized silica. *Curr. Opin. Green Sustain. Chem.* **2019**, *16*, 26–32. [[CrossRef](#)]
11. Sanz-Pérez, E.S.; Murdock, C.R.; Didas, S.A.; Jones, C.W. Direct Capture of CO<sub>2</sub> from Ambient Air. *Chem. Rev.* **2016**, *116*, 11840–11876. [[CrossRef](#)]
12. Wurzbacher, J.A.; Gebald, C.; Steinfeld, A. Separation of CO<sub>2</sub> from air by temperature-vacuum swing adsorption using diamine-functionalized silica gel. *Energy Environ. Sci.* **2011**, *4*, 3584–3592. [[CrossRef](#)]
13. Krishnamurthy, S.; Lind, A.; Bouzga, A.; Pierchala, J.; Blom, R. Post combustion carbon capture with supported amine sorbents: From adsorbent characterization to process simulation and optimization. *Chem. Eng. J.* **2021**, *406*, 127121. [[CrossRef](#)]
14. Stevens, L.; Williams, K.; Han, W.Y.; Drage, T.; Snape, C.; Wood, J.; Wang, J. Preparation and CO<sub>2</sub> adsorption of diamine modified montmorillonite via exfoliation grafting route. *Chem. Eng. J.* **2013**, *215*, 699–708. [[CrossRef](#)]
15. Raganati, F.; Chirone, R.; Ammendola, P. CO<sub>2</sub> Capture by Temperature Swing Adsorption: Working Capacity As Affected by Temperature and CO<sub>2</sub> Partial Pressure. *Ind. Eng. Chem. Res.* **2020**, *59*, 3593–3605. [[CrossRef](#)]
16. Brinker, C.J.; Scherer, G.W. CHAPTER 10—Surface Chemistry and Chemical Modification. In *Sol-Gel Science*; Brinker, C.J., Scherer, G.W., Eds.; Academic Press: San Diego, CA, USA, 1990; pp. 616–672.
17. Chen, C.; Zhang, S.; Row, K.H.; Ahn, W.-S. Amine–silica composites for CO<sub>2</sub> capture: A short review. *J. Energy Chem.* **2017**, *26*, 868–880. [[CrossRef](#)]
18. Sánchez-Vicente, Y.; Stevens, L.A.; Pando, C.; Torralvo, M.J.; Snape, C.E.; Drage, T.C.; Cabañas, A. A new sustainable route in supercritical CO<sub>2</sub> to functionalize silica SBA-15 with 3-aminopropyltrimethoxysilane as material for carbon capture. *Chem. Eng. J.* **2015**, *264*, 886–898. [[CrossRef](#)]
19. Sánchez-Vicente, Y.; Pando, C.; Cortijo, M.; Cabañas, A. Chemical surface modification of mesoporous silica SBA-15 with a tertiary aminosilane using supercritical carbon dioxide. *Microporous Mesoporous Mater.* **2014**, *193*, 145–153. [[CrossRef](#)]
20. Zemanian, T.S.; Fryxell, G.E.; Liu, J.; Mattigod, S.; Franz, J.A.; Nie, Z. Deposition of Self-Assembled Monolayers in Mesoporous Silica from Supercritical Fluids. *Langmuir* **2001**, *17*, 8172–8177. [[CrossRef](#)]
21. Cao, C.; Fadeev, A.Y.; McCarthy, T.J. Reactions of Organosilanes with Silica Surfaces in Carbon Dioxide. *Langmuir* **2001**, *17*, 757–761. [[CrossRef](#)]
22. Zhang, X.; Heinonen, S.; Levänen, E. Applications of supercritical carbon dioxide in materials processing and synthesis. *RSC Adv.* **2014**, *4*, 61137–61152. [[CrossRef](#)]
23. López-Aranguren, P.; Fraile, J.; Vega, L.F.; Domingo, C. Regenerable solid CO<sub>2</sub> sorbents prepared by supercritical grafting of aminoalkoxysilane into low-cost mesoporous silica. *J. Supercrit. Fluids* **2014**, *85*, 68–80. [[CrossRef](#)]
24. Sánchez-Vicente, Y.; Alonso-Pastor, O.; Pando, C.; Cabañas, A. Phase behaviour of the two binary systems formed by CO<sub>2</sub> and the silane precursors N-[3-(trimethoxysilyl)propyl]aniline or (3-mercaptopropyl)trimethoxysilane. *J. Chem. Thermodyn.* **2016**, *103*, 152–156. [[CrossRef](#)]
25. Tenorio, M.J.; Cabañas, A.; Pando, C.; Renuncio, J.A.R. Solubility of Pd(hfac)<sub>2</sub> and Ni(hfac)<sub>2</sub>·2H<sub>2</sub>O in supercritical carbon dioxide pure and modified with ethanol. *J. Supercrit. Fluids* **2012**, *70*, 106–111. [[CrossRef](#)]
26. Jessop, P.G.; Subramaniam, B. Gas-Expanded Liquids. *Chem. Rev.* **2007**, *107*, 2666–2694. [[CrossRef](#)]
27. Zhao, D.; Huo, Q.; Feng, J.; Chmelka, B.F.; Stucky, G.D. Nonionic Triblock and Star Diblock Copolymer and Oligomeric Surfactant Syntheses of Highly Ordered, Hydrothermally Stable, Mesoporous Silica Structures. *J. Am. Chem. Soc.* **1998**, *120*, 6024–6036. [[CrossRef](#)]



28. Shenderovich, I.G.; Buntkowsky, G.; Schreiber, A.; Gedat, E.; Sharif, S.; Albrecht, J.; Golubev, N.S.; Findenegg, G.H.; Limbach, H.-H. Pyridine-15N A Mobile NMR Sensor for Surface Acidity and Surface Defects of Mesoporous Silica. *J. Phys. Chem. B* **2003**, *107*, 11924–11939. [[CrossRef](#)]
29. Zheng, F.; Tran, D.N.; Busche, B.J.; Fryxell, G.E.; Addleman, R.S.; Zemanian, T.S.; Aardahl, C.L. Ethylenediamine-Modified SBA-15 as Regenerable CO<sub>2</sub> Sorbent. *Ind. Eng. Chem. Res.* **2005**, *44*, 3099–3105. [[CrossRef](#)]
30. Rouquerol, J.; Rouquerol, F.; Llewellyn, P.; Maurin, G.; Sing, K.S.W. *Adsorption by Powders and Porous Solids: Principles, Methodology and Applications*; Academic Press: San Diego, CA, USA, 2013.
31. Mafra, L.; Čendak, T.; Schneider, S.; Wiper, P.V.; Pires, J.; Gomes, J.R.B.; Pinto, M.L. Structure of Chemisorbed CO<sub>2</sub> Species in Amine-Functionalized Mesoporous Silicas Studied by Solid-State NMR and Computer Modeling. *J. Am. Chem. Soc.* **2017**, *139*, 389–408. [[CrossRef](#)]
32. Mafra, L.; Čendak, T.; Schneider, S.; Wiper, P.V.; Pires, J.; Gomes, J.R.B.; Pinto, M.L. Amine functionalized porous silica for CO<sub>2</sub>/CH<sub>4</sub> separation by adsorption: Which amine and why. *Chem. Eng. J.* **2018**, *336*, 612–621. [[CrossRef](#)]
33. Knöfel, C.; Descarpentries, J.; Benzaouia, A.; Zeleňák, V.; Mornet, S.; Llewellyn, P.L.; Hornebecq, V. Functionalised micro-/mesoporous silica for the adsorption of carbon dioxide. *Microporous Mesoporous Mater.* **2007**, *99*, 79–85. [[CrossRef](#)]
34. Yeo, S.-D.; Park, S.-J.; Kim, J.-W.; Kim, J.-C. Critical Properties of Carbon Dioxide + Methanol, + Ethanol, + 1-Propanol, and + 1-Butanol. *J. Chem. Eng. Data* **2000**, *45*, 932–935. [[CrossRef](#)]
35. Lim, J.S.; Lee, Y.Y.; Chun, H.S. Phase equilibria for carbon dioxide-ethanol-water system at elevated pressures. *J. Supercrit. Fluids* **1994**, *7*, 219–230. [[CrossRef](#)]
36. Joung, S.N.; Yoo, C.W.; Shin, H.Y.; Kim, S.Y.; Yoo, K.-P.; Lee, C.S.; Huh, W.S. Measurements and correlation of high-pressure VLE of binary CO<sub>2</sub>-alcohol systems (methanol, ethanol, 2-methoxyethanol and 2-ethoxyethanol). *Fluid Phase Equilib.* **2001**, *185*, 219–230. [[CrossRef](#)]
37. Matthias, T.; Katsumi, K.; Alexander, V.N.; James, P.O.; Francisco, R.-R.; Jean, R.; Kenneth, S.W.S. Physisorption of gases, with special reference to the evaluation of surface area and pore size distribution (IUPAC Technical Report). *Pure Appl. Chem.* **2015**, *87*, 1051–1069. [[CrossRef](#)]
38. Meynen, V.; Cool, P.; Vansant, E.F. Synthesis of siliceous materials with micro- and mesoporosity. *Microporous Mesoporous Mater.* **2007**, *104*, 26–38. [[CrossRef](#)]
39. Hiyoshi, N.; Yogo, K.; Yashima, T. Adsorption characteristics of carbon dioxide on organically functionalized SBA-15. *Microporous Mesoporous Mater.* **2005**, *84*, 357–365. [[CrossRef](#)]
40. Dibenedetto, A.; Aresta, M.; Fragale, C.; Narracci, M. Reaction of silylalkylmono- and silylalkyldi-amines with carbon dioxide: Evidence of formation of inter- and intra-molecular ammonium carbamates and their conversion into organic carbamates of industrial interest under carbon dioxide catalysis. *Green Chem.* **2002**, *4*, 439–443. [[CrossRef](#)]
41. Bresciani, G.; Biancalana, L.; Pampaloni, G.; Marchetti, F. Recent Advances in the Chemistry of Metal Carbamates. *Molecules* **2020**, *25*, 3603.
42. Wang, X.; Conway, W.; Lawrance, G.; Burns, R.; Puxty, G.; Maeder, M. Kinetics of the Reversible Reaction of CO<sub>2</sub>(aq) with Ammonia in Aqueous Solution. *J. Phys. Chem. A* **2011**, *115*, 6405–6412. [[CrossRef](#)]
43. Asefa, T.; Tao, Z. Mesoporous silica and organosilica materials—Review of their synthesis and organic functionalization. *Can. J. Chem.* **2012**, *90*, 1015–1031. [[CrossRef](#)]
44. Haensch, C.; Hoeppe, S.; Schubert, U.S. Chemical modification of self-assembled silane based monolayers by surface reactions. *Chem. Soc. Rev.* **2010**, *39*, 2323–2334. [[CrossRef](#)]
45. Fadeev, A.Y.; McCarthy, T.J. Self-Assembly Is Not the Only Reaction Possible between Alkyltrichlorosilanes and Surfaces: Monomolecular and Oligomeric Covalently Attached Layers of Dichloro- and Trichloroalkylsilanes on Silicon. *Langmuir* **2000**, *16*, 7268–7274. [[CrossRef](#)]
46. Tenorio, M.J.; Morère, J.; Carnerero, C.; Torralvo, M.J.; Pando, C.; Cabañas, A. Thiol group functionalization of mesoporous SiO<sub>2</sub> SBA-15 using supercritical CO<sub>2</sub>. *Microporous Mesoporous Mater.* **2018**, *256*, 147–154. [[CrossRef](#)]
47. Wei, J.; Shi, J.; Pan, H.; Zhao, W.; Ye, Q.; Shi, Y. Adsorption of carbon dioxide on organically functionalized SBA-16. *Microporous Mesoporous Mater.* **2008**, *116*, 394–399. [[CrossRef](#)]
48. Masuda, K.; Ito, Y.; Horiguchi, M.; Fujita, H. Studies on the solvent dependence of the carbamic acid formation from ω-(1-naphthyl)alkylamines and carbon dioxide. *Tetrahedron* **2005**, *61*, 213–229. [[CrossRef](#)]



49. McKittrick, M.W.; Jones, C.W. Toward single-site functional materials—Preparation of amine-functionalized surfaces exhibiting site-isolated behavior. *Chem. Mater.* **2003**, *15*, 1132–1139. [[CrossRef](#)]
50. Norihito, H.; Katsunori, Y.; Tatsuaki, Y. Adsorption of Carbon Dioxide on Amine Modified SBA-15 in the Presence of Water Vapor. *Chem. Lett.* **2004**, *33*, 510–511. [[CrossRef](#)]
51. Khatri, R.A.; Chuang, S.S.C.; Soong, Y.; Gray, M. Carbon Dioxide Capture by Diamine-Grafted SBA-15: A Combined Fourier Transform Infrared and Mass Spectrometry Study. *Ind. Eng. Chem. Res.* **2005**, *44*, 3702–3708. [[CrossRef](#)]
52. Raganati, F.; Chirone, R.; Ammendola, P. Effect of Temperature on Fluidization of Geldart's Group A and C Powders: Role of Interparticle Forces. *Ind. Eng. Chem. Res.* **2017**, *56*, 12811–12821. [[CrossRef](#)]
53. Ge, K.; Yu, Q.; Chen, S.; Shi, X.; Wang, J. Modeling CO<sub>2</sub> adsorption dynamics within solid amine sorbent based on the fundamental diffusion-reaction processes. *Chem. Eng. J.* **2019**, *364*, 328–339. [[CrossRef](#)]

**Publisher's Note:** MDPI stays neutral with regard to jurisdictional claims in published maps and institutional affiliations.



© 2020 by the authors. Licensee MDPI, Basel, Switzerland. This article is an open access article distributed under the terms and conditions of the Creative Commons Attribution (CC BY) license (<http://creativecommons.org/licenses/by/4.0/>).